

# Nuclear $\rho$ meson transparency in a relativistic Glauber model

W. Cosyn\* and J. Ryckebusch

*Department of Physics and Astronomy,*

*Ghent University, Proeftuinstraat 86, B-9000 Gent, Belgium*

(Dated: October 19, 2021)

## Abstract

**Background** The recent Jefferson Laboratory data for the nuclear transparency in  $\rho^0$  electroproduction have the potential to settle the scale for the onset of color transparency (CT) in vector meson production.

**Purpose** To compare the data to calculations in a relativistic and quantum-mechanical Glauber model and to investigate whether they are in accordance with results including color transparency given that the computation of  $\rho$ -nucleus attenuations is subject to some uncertainties.

**Method** We compute the nuclear transparencies in a multiple-scattering Glauber model and account for effects stemming from color transparency, from  $\rho$ -meson decay, and from short-range correlations (SRC) in the final-state interactions (FSI).

**Results** The robustness of the model is tested by comparing the mass dependence and the hard-scale dependence of the  $A(e, e'p)$  nuclear transparencies with the data. The hard-scale dependence of the  $(e, e'\rho^0)$  nuclear transparencies for  $^{12}\text{C}$  and  $^{56}\text{Fe}$  are only moderately affected by SRC and by  $\rho^0$ -decay.

**Conclusions** The RMSGA calculations confirm the onset of CT at four-momentum transfers of a few  $(\text{GeV}/c)^2$  in  $\rho$  meson electroproduction data. A more precise determination of the scale for the onset of CT is hampered by the lack of precise input in the FSI and  $\rho$ -meson decay calculations.

PACS numbers: 25.30.Rw, 24.85.+p, 11.80.-m

---

\*Electronic address: Wim.Cosyn@UGent.be

## I. INTRODUCTION

Color transparency (CT) is a color coherence effect that emerges from perturbative quantum chromodynamics in exclusive knockout reactions at high four-momentum transfers  $Q^2$  [1, 2]. In these reactions, a hadron is produced in a small-sized configuration (SSC) with all quarks sitting close together in the transverse plane. The color interactions with the surrounding nuclear medium cancel each other and the hadron can propagate unattenuated as the common final-state interactions (FSI) between the tagged hadron and the nuclear environment vanish. The SSC can also be produced in nonperturbative conditions [3, 4]. In this regime, the SSC evolves to its stable hadronic state over a certain formation length  $l_f$ . During its formation the hadron is subjected to reduced interactions with the nuclear medium. In order to observe a CT effect under those conditions, the formation length should be of the order of the nuclear radius ( $l_f \sim R_A$ ). Observation of the onset of CT at a certain energy scale can teach us about the cross-over point between ordinary nuclear matter and quark-gluon matter. The identification of this transition point is of great importance to nucleon-structure studies, as CT is a necessary condition for the validity of the QCD factorization theorems which are commonly applied when interpreting data [5, 6].

The measured observable in search for CT is the nuclear transparency  $T$ , defined as the ratio of the cross section per target nucleon for a process on a nucleus to the cross section of the process on a free nucleon ( $T = \sigma^A/A\sigma^N$ ). Accordingly, the nuclear transparency provides a measure of the integrated attenuation of the nuclear medium on the tagged hadrons in some (semi-)exclusive reaction. One can study the hard-scale dependence of the transparency for a certain target nucleus  $A$ , or the  $A$  dependence at a fixed value of the hard-scale parameter. If CT effects were to appear at a certain value of the hard-scale parameter, the nuclear transparency would be observed to overshoot the predictions from traditional nuclear-physics calculations. The measurement of the onset and magnitude of the CT effect allows one to constrain models describing the evolution of a SSC into a hadron.

Experimentally, CT effects have been observed in the measurement of the cross section of diffractive dissociation of 500 GeV/ $c$  pions into dijets in the E791 experiment at Fermilab [7]. At intermediate energies, no sign of CT was observed in  $A(e, e'p)$  measurements on a variety of nuclear targets and four-momentum transfers  $Q^2 \lesssim 8$  (GeV/ $c$ )<sup>2</sup> [8–14]. The nuclear  $^{12}\text{C}(p, 2p)$  transparencies were studied at Brookhaven National Laboratory (BNL)

[15–17]. The transparency first shows a rise with increasing incoming proton momentum and drops for momenta larger than 9 GeV/ $c$ . This proton-momentum dependence is at odds with traditional nuclear-physics calculations predicting  $^{12}\text{C}(p, 2p)$  nuclear transparencies which are more or less constant with proton momentum. The BNL  $^{12}\text{C}(p, 2p)$  results are currently not considered as a clean sign of CT, and competing effects stemming from nuclear filtering [18, 19] or from threshold mechanisms for charm resonance production [20] have been proposed to explain the observations.

In recent years, several experiments have measured the transparencies in semi-exclusive meson production reactions. As a meson is a more compact object than a baryon, it should be more likely to produce a meson SSC and observe the onset of CT at intermediate energies. Two recent Jefferson Laboratory (JLab) experiments that measured the transparency of pions in photo- and electroproduction [21, 22] consistently agreed with various independent calculations provided that CT effects are included [23–26]. More recently, a JLab Hall-B experiment has measured  $\rho^0$  nuclear transparencies in semi-exclusive electroproduction on  $^{56}\text{Fe}$  and  $^{12}\text{C}$  targets [27]. Again, the data agree favorably with calculations including CT effects [28, 29]. These results strengthen the case for an onset of CT at four-momentum transfers of a few  $(\text{GeV}/c)^2$  in exclusive meson production reactions. For a recent review of the CT phenomenon, see Ref. [30].

There are issues in nuclear  $\rho$  meson transparency calculations, like the absence of  $\rho N$  scattering data, which complicate the interpretation of the calculations and induce some uncertainties. It is one of the purposes of this paper to investigate these issues in more detail and to study the robustness of the computed nuclear  $\rho$  transparencies. We compare the recent  $A(e, e'\rho^0)$  transparency data with calculations in a relativistic multiple-scattering Glauber approximation (RMSGGA) model. The RMSGGA model has been used successfully to predict nuclear transparencies for  $A(e, e'p)$  reactions [31, 32], for  $A(p, 2p)$  reactions [33, 34], for  $A(\gamma, \pi^-p)$  and  $A(e, e'\pi^+)$  reactions [23, 24] and for quasi-elastic neutrino-induced processes [35]. In Sec. II we sketch the RMSGGA model while highlighting some important issues emerging for the  $\rho^0$  nuclear transparency calculations. Numerical results are shown in Sec. III for kinematics of the JLab experiment. Section IV states our conclusions.

## II. MODEL

*a. Relativistic multiple-scattering Glauber approximation* Finding its roots in optics, Glauber multiple-scattering theory [36] describes the small-angle scattering of particles in the eikonal approximation. Thereby the scattered wave function is a plane wave multiplied with an eikonal phase. The eikonal approximation is valid when the wavelength of the particle is small in comparison with the typical interaction range of the scattering particles. For baryons and mesons this criterion translates into momenta higher than a few hundred GeV/c. In Ref. [31] we have introduced a relativistic version of Glauber multiple-scattering theory. As the helicity conserving amplitude is assumed to dominate hadron-nucleon high energy scattering, the Glauber eikonal phase is a scalar in spin space. To describe multiple-rescattering the frozen approximation is used and the individual eikonal phases are multiplied. In the RMSGA model, the eikonal Glauber phase at some spatial point  $(\vec{b}, z)$  reads for the ejected  $\rho^0$

$$\mathcal{G}(\vec{b}, z) = \prod_{\alpha \neq \alpha_i} \int d\vec{r}' |\phi_\alpha(\vec{r}')|^2 \left[ 1 - \theta(z - z') \Gamma_{\rho N}(\vec{b}' - \vec{b}) \right]. \quad (1)$$

Here, the  $(\vec{b}, z)$  coordinate system has its  $z$ -axis along the  $\rho^0$  momentum,  $\phi_\alpha(\vec{r})$  are the Dirac single-particle wave functions of the residual nucleons with quantum numbers  $\alpha \equiv n\kappa m_j m_t$  obtained from the Serot-Walecka model [37], and  $\alpha_i$  characterizes the nucleon on which the  $\rho^0$  is created. The profile function  $\Gamma_{\rho N}$  in Eq. (1) is commonly described by a Gaussian

$$\Gamma_{\rho N}(\vec{b}) = \frac{\sigma_{\rho N}^{\text{tot}}(1 - i\epsilon_{\rho N})}{4\pi\beta_{\rho N}^2} \exp\left(-\frac{\vec{b}^2}{2\beta_{\rho N}^2}\right), \quad (2)$$

where  $\sigma_{\rho N}^{\text{tot}}, \epsilon_{\rho N}, \beta_{\rho N}$  are energy dependent parameters connected to  $\rho N$  scattering. Due to the lack of data for  $\rho N$  scattering it has become customary to use educated estimates for the  $\sigma_{\rho N}^{\text{tot}}, \epsilon_{\rho N}, \beta_{\rho N}$  [38] based on the corresponding values for  $\pi N$  scattering. In  $\pi N$  scattering the parameters display very little energy dependence for pion laboratory momenta  $p_\pi \gtrsim 1.5 - 2$  GeV/c and it has become customary to adopt energy-independent parameters for  $\rho N$ . In this work, we study the impact of these uncertainties for the computed nuclear  $\rho$  transparencies.

*b. Short-range correlations* The RMSGA model accommodates the possibility to include short-range correlations (SRC) in the modeling of the FSI. We use the information

that a nucleon is present at the spatial point of the hard interaction. Due to its finite size, the presence of the nucleon induces local fluctuations in the nuclear density. The inclusion of SRC in the FSI is technically achieved in the following way [24]. First, the squared single-particle wave functions in Eq. (1) can be connected to the one-body density of the target nucleus  $\rho_A^{[1]}(\vec{r})$  [normalized as  $\int d\vec{r} \rho_A^{[1]}(\vec{r}) = A$ ]

$$|\phi_\alpha(\vec{r})|^2 \approx \frac{\rho_A^{[1]}(\vec{r})}{A} = \int d\vec{r}_2 \dots \int d\vec{r}_A (\Psi_A^{\text{g.s.}}(\vec{r}, \vec{r}_2, \dots, \vec{r}_A))^\dagger \Psi_A^{\text{g.s.}}(\vec{r}, \vec{r}_2, \dots, \vec{r}_A). \quad (3)$$

Here,  $\Psi_A^{\text{g.s.}}$  is the ground-state wave function of the target nucleus, obtained by antisymmetrizing the product of the single-particle wave functions  $\phi_\alpha$ . Even in a small nucleus like  ${}^4\text{He}$ , the above approximation (better known as the thickness approximation) marginally affects the predicted effect of FSI [31]. In a second step, the averaged density  $\rho_A^{[1]}(\vec{r})$  can be substituted with the ratio of the two-body density  $\rho_A^{[2]}$  (normalized as  $\int d\vec{r}_1 \int d\vec{r}_2 \rho_A^{[2]}(\vec{r}_1, \vec{r}_2) = A(A-1)$ ) and the one-body density:

$$\rho_A^{[1]}(\vec{r}) \rightarrow \frac{A}{A-1} \frac{\rho_A^{[2]}(\vec{r}, \vec{r}_1)}{\rho_A^{[1]}(\vec{r}_1)}, \quad (4)$$

where  $\vec{r}_1$  is the spatial coordinate corresponding with the hard interaction. One can include SRC in the two-body density by adopting the functional form [39]:

$$\rho_A^{[2]}(\vec{r}_1, \vec{r}_2) \approx \frac{A-1}{A} \gamma(\vec{r}_1) \rho_A^{[1]}(\vec{r}_1) \rho_A^{[1]}(\vec{r}_2) \gamma(\vec{r}_2) g(r_{12}), \quad (5)$$

where  $g(r_{12})$  is the Jastrow correlation function [40] and  $\gamma(\vec{r})$  a function that imposes the normalization of the two-body density obtained as the solution of an integral equation. With the above expression for the SRC-corrected two-body density, Eq. (4) becomes

$$\rho_A^{[1]}(\vec{r}) \rightarrow \gamma(\vec{r}) \rho_A^{[1]}(\vec{r}) \gamma(\vec{r}_1) g(|\vec{r} - \vec{r}_1|) \equiv \rho_A^{\text{eff}}(\vec{r}, \vec{r}_1). \quad (6)$$

In summary, the FSI calculations can be corrected for SRC by replacing  $|\phi_\alpha(\vec{r})|^2$  with  $\rho_A^{\text{eff}}(\vec{r}, \vec{r}_1)/A$  in Eq. (1). To illustrate the effectiveness and robustness of the RMSGA model in describing a variety of knockout reactions, we show in Fig. 1 RMSGA predictions for the  $A(e, e'p)$  nuclear transparencies and compare them to the published data. Neither the calculations nor the data include the commonly applied (and rather arbitrary) correction factors  $c_A$  that account for shifts in the nuclear spectral function to higher missing momenta and energies due to SRC. For a discussion on this subject, we refer to Ref. [30]. We observe

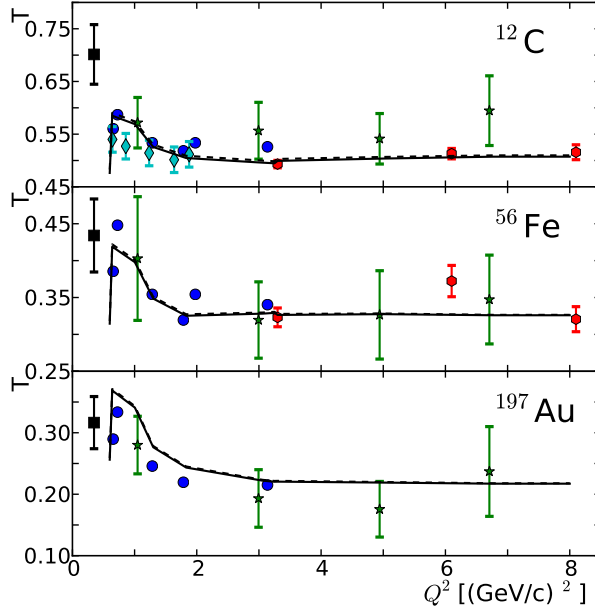


FIG. 1: (Color online) Nuclear transparencies versus  $Q^2$  for  $A(e, e'p)$  reactions in quasi-elastic kinematics. Solid black lines are RMSGGA calculations with the Glauber phase of Eq. (1). Dashed black lines show the RMSGGA calculations corrected for SRC according to the replacement of Eq. (6) in Eq. (1). Data are from Refs. [8] (black squares), [9, 10] (red hexagons), [12] (green stars), [14] (cyan diamonds), and [11, 13] (blue circles). Data and calculations do not include the  $c_A$  factor applied in [32].

an excellent agreement between the RMSGGA calculations and the world data on  $A(e, e'p)$  nuclear transparencies. Both the hard-scale  $Q^2$  dependence and the mass dependence of the data are nicely predicted. Inclusion of the SRC in the FSI enhances the  $T$  by a tiny amount. The biggest enhancement is of the order of 0.5% and is observed for the lowest  $Q^2$  values of the  $^{12}\text{C}$  transparency. It is noteworthy to mention that the  $A(e, e'\rho^0)$  calculations presented below use identical nuclear-structure input as used for the  $A(e, e'p)$ .

*c. Color transparency* The effects of color transparency are implemented by means of the quantum diffusion model of Ref. [41]. Thereby, the position independent parameter  $\sigma_{\rho N}^{\text{tot}}$  in the profile function of Eq. (2) is replaced by a position-dependent effective one  $\sigma_{\rho N}^{\text{eff}}(\mathcal{Z})$  which evolves in a linear fashion along the formation length  $l_f$  from a reduced value for the

SSC to the standard one associated with the normal hadron

$$\sigma_{\rho N}^{\text{eff}}(\mathcal{Z}) = \sigma_{\rho N}^{\text{tot}} \left\{ \left[ \frac{\mathcal{Z}}{l_f} + \frac{\langle n^2 k_t^2 \rangle}{\mathcal{H}} \left( 1 - \frac{\mathcal{Z}}{l_f} \right) \right] \theta(l_f - \mathcal{Z}) + \theta(\mathcal{Z} - l_f) \right\}. \quad (7)$$

Here,  $n$  is the number of elementary fields ( $n = 2$  for the  $\rho^0$ ),  $k_t = 0.350$  GeV/ $c$  is the average transverse momentum of a quark inside a hadron,  $\mathcal{Z}$  is the distance from the hard interaction point  $\vec{r}_1$  along the ejected hadron path, and  $\mathcal{H} \equiv Q^2$  is the hard-scale parameter that governs the CT effect. Unless otherwise stated, for the formation length  $l_f \approx 2p/\Delta M^2$ , we adopt the value  $\Delta M^2 = 0.7$  (GeV/ $c^2$ )<sup>2</sup>. With this value we could reproduce the measured nuclear pion transparencies [22].

*d.  $\rho$  decay* The  $\rho^0$  decays to a pair of pions with a branching ratio of almost 99%. For the kinematics of the JLab experiment the average life time of the  $\rho^0$  corresponds to a mean path length of about 5 fm. This means that the majority of the  $\rho^0$  will decay outside the nuclear medium and the anticipated effect on the computed nuclear transparencies is rather modest. The average opening angle of the pion pair is around 30 degrees in the laboratory frame. Therefore, it is fair to substitute the  $\sigma_{\rho N}^{\text{tot}}$  in Eq. (2) by  $(\sigma_{\pi^- N}^{\text{tot}} + \sigma_{\pi^+ N}^{\text{tot}})$  after the decay. The  $\rho^0$  decay is expected to lower the nuclear transparency as the pion pair is subject to an increased attenuation compared to the  $\rho^0$ . The adopted procedure gives an upper limit for the effect of  $\rho$  decay as it adds the attenuation on the two pions in an incoherent way by making them move collinearly [24]. We include the effect of  $\rho^0$  decay by replacing the  $\rho N$  total cross section  $\sigma_{\rho N}^{\text{tot}}$  in Eq. (2) by a position dependent one

$$\sigma_{\text{decay}}^{\text{tot}}(\mathcal{Z}) = \sigma_{\rho N}^{\text{tot}} e^{-Z\Gamma_\rho \sqrt{1-|\vec{p}_\rho|^2/E_\rho^2}} + (\sigma_{\pi^- N}^{\text{tot}} + \sigma_{\pi^+ N}^{\text{tot}})(1 - e^{-Z\Gamma_\rho \sqrt{1-|\vec{p}_\rho|^2/E_\rho^2}}). \quad (8)$$

Here,  $\vec{p}_\rho$  ( $E_\rho$ ) are the rho meson momentum (energy), and  $\Gamma_\rho = 149$  MeV is the  $\rho^0$  decay width in the laboratory frame.

*e. Cross section* The cross section for  $\rho^0$  electroproduction on a nucleus  $A$  ( $e + A \rightarrow e' + \rho^0 + A^*$ ) takes the following form (Dirac spinors are normalized as  $\bar{u}u = 1$ )

$$\frac{d\sigma^{eA}}{dE_{e'} d\Omega_{e'} dt d\phi_\rho} = \sum_\alpha \frac{\alpha_{\text{EM}}}{8(2\pi)^4} \frac{E_{e'}}{qE_e Q^2 (1-\epsilon)} \overline{\sum} |\mathcal{M}_\alpha^{\gamma^* A}|^2. \quad (9)$$

Here, the summation runs over all the shells  $\alpha$  of the nucleus  $A$ ,  $E_e$  and  $E_{e'}$  are incoming and scattered electron energy,  $\alpha_{\text{EM}}$  is the fine structure constant, the virtual photon  $q^\mu(\nu, \vec{q})$  has four-momentum transfer  $Q^2 = -q^2$  and degree of transverse polarization  $\epsilon$ ,  $t = (q - p_\rho)^2$ ,  $\overline{\sum}$  denotes the summing and averaging over spin degrees of freedom, and  $\mathcal{M}^{\gamma^* A}$  is the matrix

element of the  $\gamma^* + A \rightarrow \rho^0 + A^*$  reaction (with  $A^*$  the residual nucleus) for  $\gamma^*$  absorption on a nucleon with quantum numbers  $\alpha$ . In a factorized approach, the squared matrix element can be approximated as [24, 33]

$$\overline{\sum} |\mathcal{M}^{\gamma^* A}|^2 \approx \int d\vec{p}_m \overline{\sum} |\mathcal{M}^{\gamma^* N}|^2 \rho_\alpha^D(\vec{p}_m), \quad (10)$$

where  $\mathcal{M}^{\gamma^* N}$  is the amplitude of the  $\gamma^* + N \rightarrow \rho^0 + N$  process,  $\vec{p}_m = \vec{p}_\rho - \vec{q}$  is the missing momentum, and the distorted momentum distribution  $\rho_\alpha^D$  is defined as

$$\rho_\alpha^D(\vec{p}_m) = \frac{1}{(2\pi)^3} \sum_{m_j, m_s} \left| \int d\vec{r} e^{-i\vec{p}_m \cdot \vec{r}} \mathcal{G}(\vec{b}, z) \bar{u}(\vec{p}_m, m_s) \phi_\alpha(\vec{r}) \right|^2. \quad (11)$$

In Eq.(10), the matrix element can be related to the cross section in the center-of-mass frame:

$$\frac{d\sigma^{\gamma^* N}}{d|t|d\phi^*} = \frac{m_N^2}{8\pi^2(s^2 - 2s(m_N^2 - Q^2) + (m_N^2 + Q^2)^2)} \overline{\sum} \mathcal{M}^{\gamma^* N} \approx \left( \frac{d\sigma}{d|t|} \right)_0 e^{-\beta_{\gamma\rho} t}, \quad (12)$$

where  $s = W^2$ , the squared c.m. energy for the  $\gamma^* N$  system. In the last step we made use of the diffractive properties of the vector meson cross section at GeV energies. For the slope factor of the diffractive  $\rho^0$  production, we take  $\beta_{\gamma\rho} = 6 \text{ (GeV}/c)^{-2}$  [38, 42–44] and leave  $\left( \frac{d\sigma}{d|t|} \right)_0$  unspecified as it cancels in the nuclear transparency ratio  $T = \sigma^A/A\sigma^N$ . Combining Eqs. (9), (10) and (12) gives us the following formula for the cross section:

$$\begin{aligned} \frac{d\sigma^{eA}}{dE_{e'} d\Omega_{e'} dt d\phi_\rho} &= \sum_\alpha \int d\vec{p}_m \frac{\alpha_{\text{EM}}}{4(2\pi)^2} \\ &\times \frac{E_{e'} \rho_\alpha^D(\vec{p}_m) [s^2 - 2s(m_N^2 - Q^2) + (m_N^2 + Q^2)^2]}{q E_e Q^2 (1 - \epsilon) m_N^2} \left( \frac{d\sigma}{d|t|} \right)_0 e^{-\beta_{\gamma\rho} t}. \end{aligned} \quad (13)$$

### III. RESULTS

The JLab Hall-B experiment E02-110 measured the nuclear transparency in  $\rho^0$  electroproduction for  $0.8 \leq Q^2 \leq 3 \text{ (GeV}/c)^2$  on  $^{12}\text{C}$  and  $^{56}\text{Fe}$  targets using the CLAS  $4\pi$  detector. In order to select elastically produced  $\rho^0$  mesons and suppress pions from resonance decays the following kinematical cuts were imposed:  $z(= E_\rho/\nu) > 0.9$  and  $W > 2 \text{ GeV}$ . To ensure the selection of exclusive diffractive and incoherent events,  $t$  was limited to  $-0.4 < t < -0.1 \text{ (GeV}/c)^2$ . In vector meson electroproduction, the virtual photon will fluctuate into a  $q\bar{q}$  pair along a certain coherence length  $l_c = 2\nu/(Q^2 + m_{q\bar{q}}^2)$  and then scatter off a nucleon. To



isolate a possible CT signal it is essential that  $l_c$  is more or less constant over the kinematic ranges included in the analysis. As the  $q\bar{q}$  is subject to initial-state interactions (ISI), a variation in  $l_c$  can cause a change in the transparency and thus mimic a CT signal. For the JLab experiment E02-110 one has  $0.5 \leq l_c \leq 0.8$  fm. This is sufficiently smaller than the typical intra-nucleon distance in the nucleus, so ISI are not included in our calculations.

The nuclear transparencies shown here are computed as the ratio of the cross section of Eq. (13) to its plane-wave approximation (PWA) equivalent. The PWA cross section neglects any form of FSI and is obtained by putting  $\mathcal{G} = 1$  in Eq. (11). It deserves highlighting that the experimentally extracted nuclear  $\rho$  transparencies use a ratio of the phase-space integrated cross sections from nucleus  $A$  to the deuteron. In Ref. [29] it is pointed out that Fermi motion can introduce an overall change in the transparency with a constant factor and mimic part of a CT signal through a  $Q^2$  dependent change of the plane-wave ratio. The results of Ref. [29] suggest that in the PWA the ratio of the cross section on  $A$  relative to the deuteron increases with  $Q^2$  due to the applied cuts in  $t$  and the effect of Fermi motion. For the calculations presented here we prefer to compute the transparencies as a ratio of the RMSGA to the PWA cross sections for  $^{12}\text{C}$  and  $^{56}\text{Fe}$ . Indeed, the nuclear transparency computed as a RMSGA/PWA ratio for the same target nucleus is less prone to errors stemming from specific phase-space mismatches between  $^{12}\text{C}$ ,  $^{56}\text{Fe}$  and the deuteron for example, as well as other uncertainties as possible medium-effects on the  $\gamma^* + N \rightarrow \rho + N$  reaction amplitude.

The experimental kinematical cuts determine the phase space of the calculations. For each  $Q^2$  bin, we fix  $Q^2$  at its central value and compute the RMSGA and PWA cross sections for the ranges in  $(\nu, z, t)$  used in the analysis of the data. The final result for the nuclear transparency at a particular value of the hard-scale parameter  $Q^2$  is computed as the ratio of the integrated RMSGA cross section to the integrated PWA one, whereby both in the nominator and the denominator the same ranges in  $(\nu, z, t)$  are considered.

Figure 2 shows the hard-scale dependence of the RMSGA nuclear  $^{12}\text{C}(e, e'\rho^0)$  transparencies for  $\sigma_{\rho N}^{\text{tot}}=25$  mb,  $\beta_{\rho N} = 6$  (GeV/c) $^{-2}$ ,  $\epsilon_{\rho N} = -0.2$  taken constant as a function of energy. We investigate the hard-scale dependence stemming from the effect of CT,  $\rho$  decay, and SRC. The computed transparencies that do not include CT show little dependence on  $Q^2$  as can be anticipated from the energy independence of the Glauber scattering parameters at these energies. The SRC component in the FSI adds about 0.5% to the transparency, independent

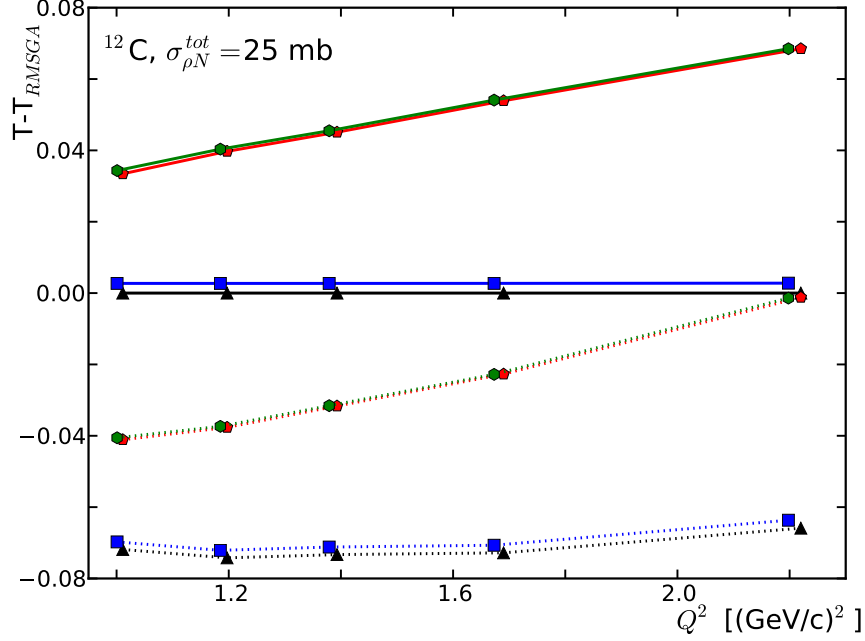


FIG. 2: (Color online) Relative effect of the SRC, of the  $\rho$ -decay, and of the CT on the predicted hard-scale dependence of the  $^{12}\text{C}(e, e'\rho^0)$  nuclear transparencies. All calculations use  $\sigma_{\rho N}^{\text{tot}}=25$  mb and  $\beta_{\rho N} = 6$   $(\text{GeV}/c)^{-2}$ . Base-line calculations (denoted as  $T_{\text{RMSG}_A}$ ) are obtained with Eqs. (1) and (2). Dashed (solid) curves include (exclude) the effect of  $\rho$  decay implemented with the Eq. (8). Black triangles (blue squares) exclude (include) the effect of SRC in the computation of the FSI. Green pentagrams include the effect of CT and red hexagons include both SRC and CT. Some points are offset on the  $x$ -axis for clarity. The kinematic cuts are those of the JLab E02-110 experiment (details in text).

of the value of the hard scale parameter. Accordingly, the CT and SRC mechanisms can be separated by studying the hard-scale dependence of the transparency. The  $\rho$  decay lowers the transparency with about 7% at the lowest  $Q^2$  data point and 6% at the highest  $Q^2$  data point, reflecting the longer dilated  $\rho$  half-life time at higher energies. The CT effects induce the strongest  $Q^2$  dependence, increasing the transparency with 3 to 6% from low to high  $Q^2$ . The inclusion of SRC in the FSI for the CT calculations yields almost no increase of the transparency as the produced  $\rho^0$  in the SSC is already subjected to reduced interactions in the local neighborhood of the hard interaction where also the SRC effectively modify the density.

Figures 3 and 4 compare the RMSGA transparencies including SRC and  $\rho$  decay with the

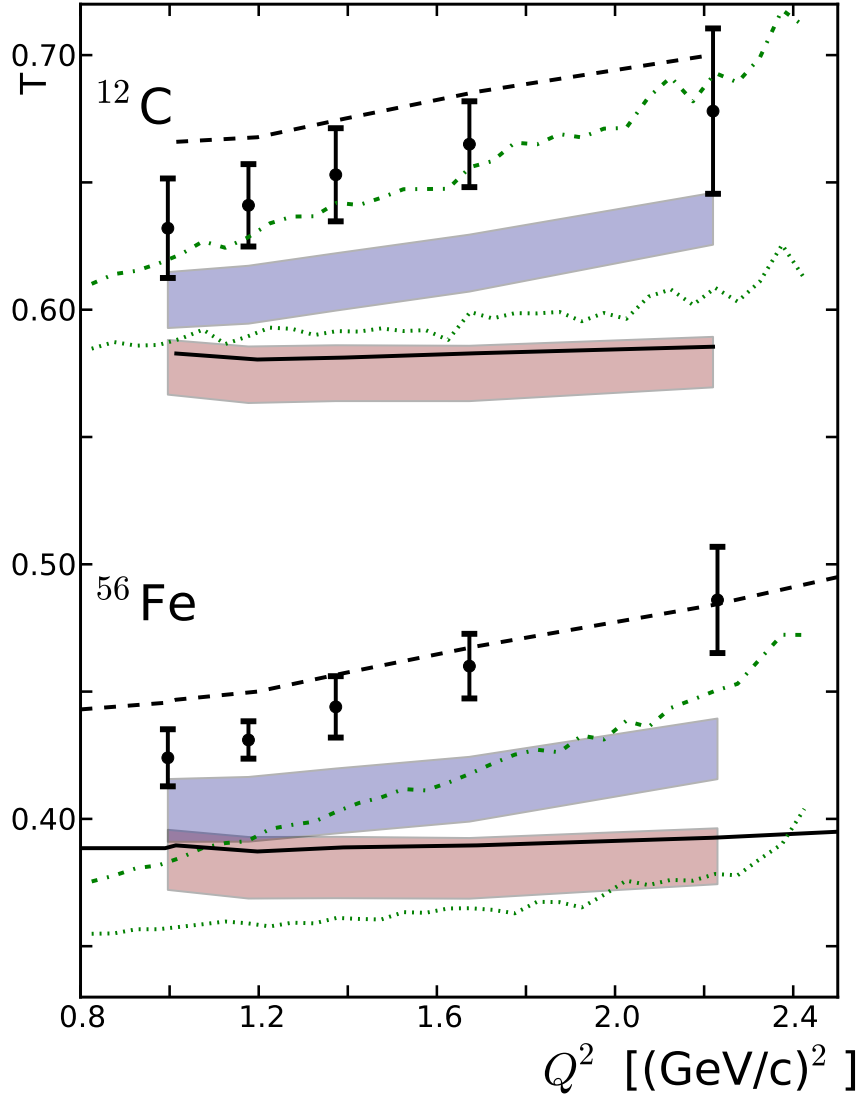


FIG. 3: (Color online) Nuclear transparency for  $\rho$  electroproduction as a function of  $Q^2$  in  $^{12}\text{C}$  and  $^{56}\text{Fe}$  with  $\sigma_{\rho N}^{\text{tot}} = 20$  mb. Data are from [27]. Black curves are calculations from the model of Ref. [28] with (dashed) and without (full) CT effects. Green curves are calculations from the model of Ref. [29] with (dash-dotted) and without (dotted) CT effects. Blue (with CT effects) and red (no CT effects) shaded bands are results from the RMSGA model including rho decay and SRC effects.

JLab data. Given the lack of detailed information on the  $\sigma_{\rho N}^{\text{tot}}$  parameter, we show results of calculations for  $\sigma_{\rho N}^{\text{tot}} = 20$  mb (Fig. 3), and for  $\sigma_{\rho N}^{\text{tot}} = 25$  mb (Fig. 4). As mentioned in Sec. II the computed transparencies including the decay of the  $\rho$  meson by means of

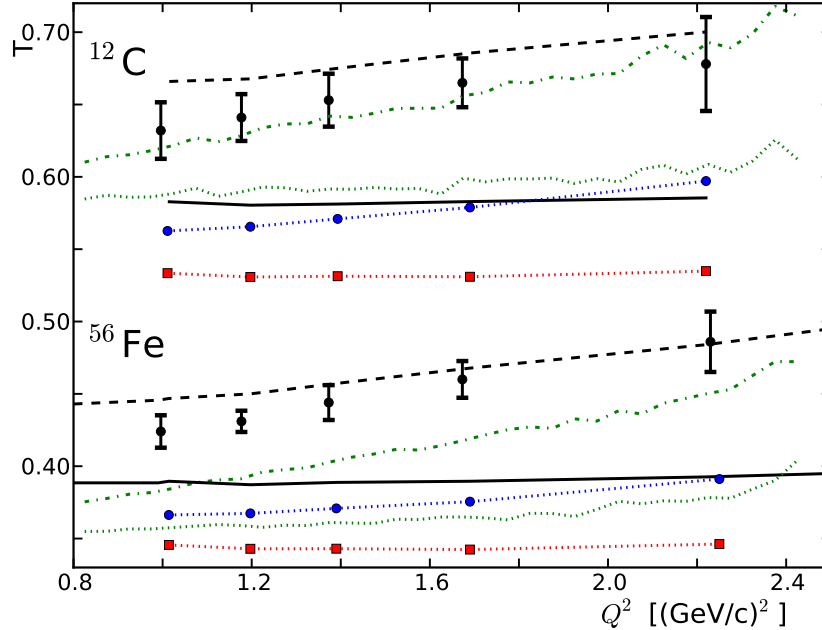


FIG. 4: (Color online) As in Fig. 3 but for  $\sigma_{\rho N}^{\text{tot}} = 25$  mb. Blue circles (with CT effects) and red squares (no CT effects) curves are results from the RMSGA model including rho decay and SRC effects.

Eq. (8) represent a lower limit. We therefore have chosen to represent our calculations in Fig. 3 as a shaded region, confined on the lower side by the calculations with the  $\rho$  meson decay evaluated with the expression for the  $\rho N$  total cross section of Eq. (8) which assumes that the two pions move collinearly. We have also evaluated the transparency of two pions decaying from a 3 GeV  $\rho$  meson (representative for the kinematics of the data) with various  $\pi - \rho$  c.o.m. angles and have compared this to value of the transparency for two collinear pions. We find a maximum enhancement of the two-pion transparency of 28% for  $^{12}\text{C}$  and 20% for  $^{56}\text{Fe}$  compared to the collinear situation. The upper limits of the bands in Fig. 3 are obtained by reducing the effect of the inclusion of rho meson decay by 28% for  $^{12}\text{C}$  and 20% for  $^{56}\text{Fe}$ . This is a fair estimate of the maximum impact of the incoherence effect. Therefore, the width of the band reflects the estimated uncertainty in the computation of the effect of the  $\rho^0$  decay. In Fig. 4 we only show the curves corresponding with the lower limit of the bands in order to compare to alternate model calculations.

Figures 3 and 4 also include two other model calculations. The model by Frankfurt, Miller, and Strikman (FMS) [28] is based on a semi-classical Glauber calculation and implements

the effects of CT and  $\rho$  decay along similar lines as ours, with the values of  $\sigma_{\rho N}^{\text{tot}}=25$  mb,  $\Delta M^2 = 0.7$  (GeV/c<sup>2</sup>)<sup>2</sup>, and  $\Gamma_\rho = 149$  MeV. The calculations of Ref. [29] from the Giessen group include a model for the elementary  $\rho$  production and describe the FSI with the semi-classical GiBUU transport model [45, 46]. Given their very different nature, it is satisfying that all three models yield similar <sup>12</sup>C transparencies when ignoring CT. The predictions including CT effects show a little more variation over the different groups, but display similar trends in their  $Q^2$  dependence. At identical parameter input in the Glauber part, we obtain a transparency that is about 5% lower than those of the FMS model. The difference between the calculations including and excluding CT effects is also bigger in the FMS model. It is worth noting that when considering the  $A$ -dependence, none of the models can satisfyingly describe the data for both nuclei with the same parameter set. This was not the case for the  $A(e, e'p)$  and  $A(e, e'\pi^+)$  data, where one parameter set gave a very good agreement over the whole measured  $A$ -range. The RMSGA results with  $\sigma_{\rho N}^{\text{tot}} = 20$  mb are a better match for the data than those with  $\sigma_{\rho N}^{\text{tot}} = 25$  mb, but are underestimating both the magnitude and the  $Q^2$  slope of the data.

In the quantum diffusion CT model of Eq. (7) the CT effect can be made bigger by decreasing the value of  $\Delta M^2$ . Up to this point,  $\Delta M^2 = 0.7$  (GeV/c<sup>2</sup>)<sup>2</sup> has been used. To date, however, there is little guidance with regard to realistic ranges for those parameters. In Fig. 5 we show calculations for three different  $\Delta M^2$  values. The  $\Delta M^2 = 1$  (GeV/c<sup>2</sup>)<sup>2</sup> corresponds with the value commonly adopted for the nucleon. It is clear that the results with  $\Delta M^2 = 0.5$  (GeV/c<sup>2</sup>)<sup>2</sup> yield the best correspondence with the data, both with regard to the magnitudes and  $Q^2$  slope. Any further fine tuning of the parameters is not opportune given the mentioned uncertainties in the calculations.

In Table III we assess the computed and measured slopes of the hard-scale dependence of the rho transparencies. We clearly see a better agreement between the measured slopes and those calculations including CT. As becomes clear from Fig. 3 the FMS and RMSGA calculations with  $\Delta M^2 = 0.7$  (GeV/c<sup>2</sup>)<sup>2</sup> tend to underestimate the measured slopes. While the computed slope with  $\Delta M^2 = 0.5$  (GeV/c<sup>2</sup>)<sup>2</sup> is within the error bars for <sup>12</sup>C, it is substantially underestimating the measured <sup>56</sup>Fe one. The GiBUU predictions show a stronger  $Q^2$  dependence than our calculations. This can be explained by the effect of Fermi motion in large nuclei mentioned earlier in this section, which induces an additional rise in  $T$  with  $Q^2$  on top of the one due to the CT effect.

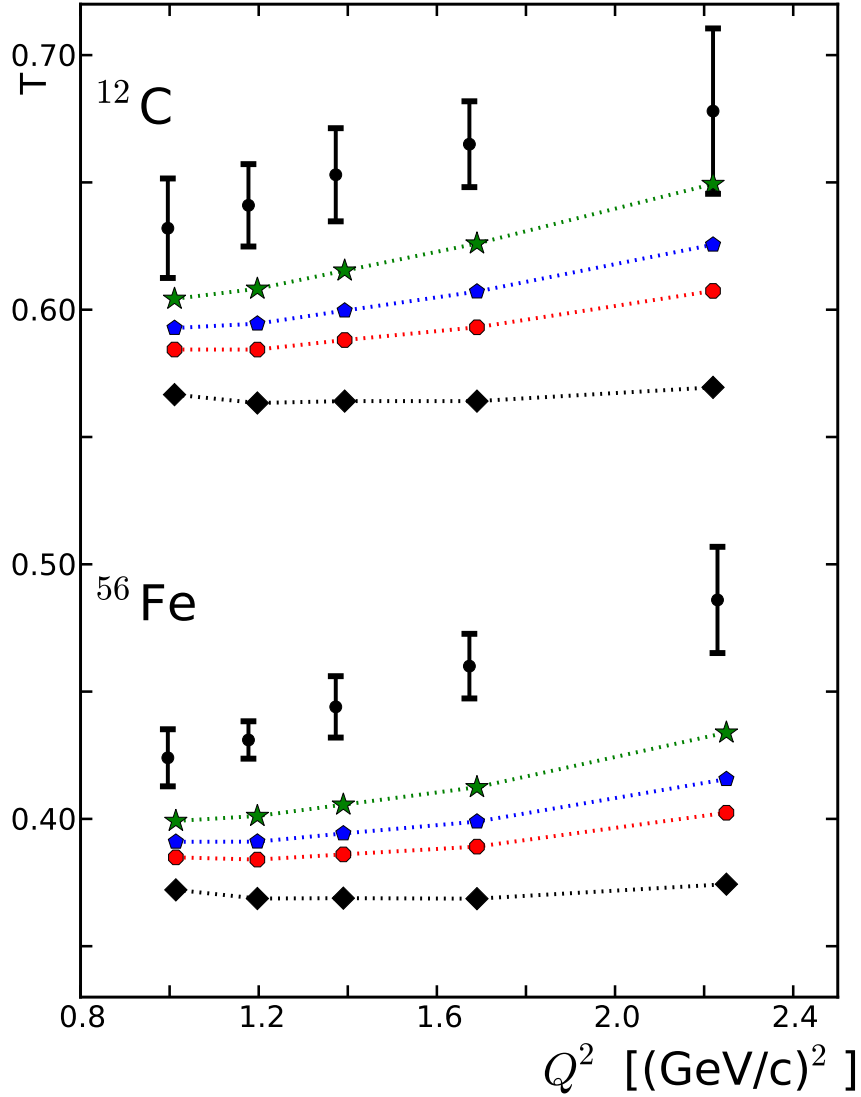


FIG. 5: (Color online) The hard-scale dependence of the nuclear rho transparencies for  $\sigma_{\rho N}^{\text{tot}} = 20$  mb and various choices of the formation length:  $\Delta M^2 = 0.5$  (GeV/c $^2$ ) $^2$  (green stars),  $\Delta M^2 = 0.7$  (GeV/c $^2$ ) $^2$  (blue pentagrams) and  $\Delta M^2 = 1.0$  (GeV/c $^2$ ) $^2$  (red circles). The black diamonds curve does not include CT effects. All curves include the  $\rho$ -meson decay and SRC effects.

#### IV. CONCLUSION

We have performed relativistic Glauber calculations for  $A(e, e'\rho^0)$  transparencies and compared them to the recent JLab data. The effects of short-range correlations, color transparency, and the decay of the  $\rho$  meson to a pair of pions can be included. The covered phase space in the calculations matches the experimental conditions and all kinematical

nucleus	$\sigma_{\rho N}^{\text{tot}}$ [mb]	$\Delta M^2$ (GeV/c <sup>2</sup> ) <sup>2</sup>	JLab data [27]	RMSGGA (+SRC +CT+decay)	RMSGGA (+SRC+CT)	RMSGGA (+SRC+decay)	RMSGGA (+SRC)
<sup>12</sup> C	25	0.5	0.044± 0.015 ± 0.019	0.040	0.034	0.0017	-0.0038
<sup>12</sup> C	25	0.7		0.029	0.024	0.0017	-0.0038
<sup>12</sup> C	25	1.0		0.020	0.016	0.0017	-0.0038
<sup>12</sup> C	20	0.5	0.044± 0.015 ± 0.019	0.038	0.030	0.0032	-0.0037
<sup>12</sup> C	20	0.7		0.028	0.021	0.0032	-0.0037
<sup>12</sup> C	20	1.0		0.020	0.014	0.0032	-0.0037
<sup>56</sup> Fe	25	0.5	0.053 ± 0.008± 0.013	0.029	0.026	0.0011	-0.0050
<sup>56</sup> Fe	25	0.7		0.020	0.017	0.0011	-0.0050
<sup>56</sup> Fe	25	1.0		0.014	0.011	0.0011	-0.0050
<sup>56</sup> Fe	20	0.5	0.053 ± 0.008± 0.013	0.029	0.025	0.0026	-0.0050
<sup>56</sup> Fe	20	0.7		0.021	0.016	0.0026	-0.0050
<sup>56</sup> Fe	20	1.0		0.015	0.010	0.0026	-0.0050

TABLE I: Slopes for the hard scale dependence of the  $\rho$  nuclear transparencies. Different RMSGGA calculations are compared to the JLab data.

cuts are taken into account. The predicted effect of SRC in the final-state interactions on the computed transparencies is small, or even negligible after also including CT effects. Including the  $\rho$  meson decay lowers the transparency up to 6-7 %, with a smaller decrease for higher  $Q^2$ . This reflects the higher absorption rate of the two pions compared to the  $\rho$ .

When comparing to the data and other model calculations, the results including the CT effect are consistently in better agreement than those without. The data suggest a stronger hard-scale dependence of the transparencies than predicted by our calculations using educated estimates for the parameters determining the magnitude of the CT effect. The presented comparison between calculations and data, gives additional support for the onset of CT in meson electroproduction reactions at energies of a few (GeV/c)<sup>2</sup>.

## ACKNOWLEDGMENTS

The authors are thankful to Lamiaa El Fassi for useful discussions. The computational resources (Stevin Supercomputer Infrastructure) and services used in this work were provided by Ghent University, the Hercules Foundation and the Flemish Government department EWI. This work is supported by the Research Foundation Flanders.

---

- [1] S. J. Brodsky, G. T. Bodwin, and G. P. Lepage, Proceedings of the 13th Int. Symp. on Multiparticle Dynamics, Volendam p. 963 (1982).
- [2] A. Mueller, Proceedings of the Seventeenth Rencontre de Moriond, Moriond p. 13 (1982).
- [3] L. Frankfurt, G. Miller, and M. Strikman, Comments Nucl.Part.Phys. **21**, 1 (1992).
- [4] L. Frankfurt, G. A. Miller, and M. Strikman, Nucl. Phys. **A555**, 752 (1993).
- [5] L. Frankfurt, G. A. Miller, and M. Strikman, Phys. Rev. **D65**, 094015 (2002), hep-ph/0010297.
- [6] J. C. Collins, L. Frankfurt, and M. Strikman, Phys. Rev. **D56**, 2982 (1997), hep-ph/9611433.
- [7] E. M. Aitala, S. Amato, J. C. Anjos, J. A. Appel, D. Ashery, S. Banerjee, I. Bediaga, G. Blaylock, S. B. Bracker, P. R. Burchat, et al. (Fermilab E791 Collaboration), Phys. Rev. Lett. **86**, 4773 (2001), hep-ex/0010044.
- [8] G. Garino, M. Saber, R. E. Segel, D. F. Geesaman, R. Gilman, M. C. Green, R. J. Holt, J. P. Schiffer, B. Zeidman, E. J. Beise, et al., Phys. Rev. C **45**, 780 (1992).
- [9] N. C. R. Makins, R. Ent, M. S. Chapman, J.-O. Hansen, K. Lee, R. G. Milner, J. Nelson, R. G. Arnold, P. E. Bosted, C. E. Keppel, et al., Phys. Rev. Lett. **72**, 1986 (1994).
- [10] T. O'Neill, W. Lorenzon, P. Anthony, R. Arnold, J. Arrington, E. Beise, J. Belz, P. Bosted, H.-J. Bulten, M. Chapman, et al., Phys. Lett. **B351**, 87 (1995), hep-ph/9408260.
- [11] D. Abbott, A. Ahmidouch, T. A. Amatuoni, C. Armstrong, J. Arrington, K. A. Assamagan, K. Bailey, O. K. Baker, S. Barrow, K. Beard, et al., Phys. Rev. Lett. **80**, 5072 (1998).
- [12] K. Garrow, D. McKee, A. Ahmidouch, C. S. Armstrong, J. Arrington, R. Asaturyan, S. Avery, O. K. Baker, D. H. Beck, H. P. Blok, et al., Phys. Rev. C **66**, 044613 (2002), hep-ex/0109027.
- [13] D. Dutta, D. van Westrum, D. Abbott, A. Ahmidouch, T. A. Amatuoni, C. Armstrong, J. Arrington, K. A. Assamagan, K. Bailey, O. K. Baker, et al. (Jefferson Lab E91013), Phys. Rev. C **68**, 064603 (2003), nucl-ex/0303011.



- [14] D. Rohe, O. Benhar, C. S. Armstrong, R. Asaturyan, O. K. Baker, S. Bueltmann, C. Carasco, D. Day, R. Ent, H. C. Fenker, et al. (E97-006 Collaboration), Phys. Rev. C **72**, 054602 (2005), nucl-ex/0506007.
- [15] A. S. Carroll, D. S. Barton, G. Bunce, S. Gushue, Y. I. Makdisi, S. Heppelmann, H. Courant, G. Fang, K. J. Heller, M. L. Marshak, et al., Phys. Rev. Lett. **61**, 1698 (1988).
- [16] I. Mardor, S. Durrant, J. Aclander, J. Alster, D. Barton, G. Bunce, A. Carroll, N. Christensen, H. Courant, S. Gushue, et al., Phys. Rev. Lett. **81**, 5085 (1998).
- [17] A. Leksanov, J. Alster, G. Asryan, Y. Averichev, D. Barton, V. Baturin, N. Bukhtoyarova, A. Carroll, S. Heppelmann, T. Kawabata, et al., Phys. Rev. Lett. **87**, 212301 (2001), hep-ex/0104039.
- [18] J. P. Ralston and B. Pire, Phys. Rev. Lett. **61**, 1823 (1988).
- [19] J. P. Ralston and B. Pire, Phys. Rev. Lett. **65**, 2343 (1990).
- [20] S. J. Brodsky and G. F. de Teramond, Phys. Rev. Lett. **60**, 1924 (1988).
- [21] D. Dutta, F. Xiong, L. Y. Zhu, J. Arrington, T. Averett, E. Beise, J. Calarco, T. Chang, J. P. Chen, E. Chudakov, et al. (Jefferson Lab E940104 Collaboration), Phys. Rev. **C68**, 021001 (2003), nucl-ex/0305005.
- [22] B. Clasie et al., Phys. Rev. Lett. **99**, 242502 (2007), 0707.1481.
- [23] W. Cosyn, M. C. Martinez, J. Ryckebusch, and B. Van Overmeire, Phys. Rev. **C74**, 062201 (2006), nucl-th/0701029.
- [24] W. Cosyn, M. C. Martinez, and J. Ryckebusch, Phys. Rev. **C77**, 034602 (2008), 0710.4837.
- [25] A. Larson, G. A. Miller, and M. Strikman, Phys. Rev. **C74**, 018201 (2006), nucl-th/0604022.
- [26] M. M. Kaskulov, K. Gallmeister, and U. Mosel, Phys. Rev. **C79**, 015207 (2009), 0808.2564.
- [27] L. El Fassi, L. Zana, K. Hafidi, M. Holtrop, B. Mustapha, et al., Phys. Lett. **B712**, 326 (2012), 1201.2735.
- [28] L. Frankfurt, G. A. Miller, and M. Strikman, Phys. Rev. **C78**, 015208 (2008), 0803.4012.
- [29] K. Gallmeister, M. Kaskulov, and U. Mosel, Phys. Rev. **C83**, 015201 (2011), 1007.1141.
- [30] D. Dutta, K. Hafidi, and M. Strikman, Prog.Part.Nucl.Phys. **69**, 1 (2013), 1211.2826.
- [31] J. Ryckebusch, D. Debruyne, P. Lava, S. Janssen, B. Van Overmeire, and T. Van Cauteren, Nucl. Phys. **A728**, 226 (2003), nucl-th/0305066.
- [32] P. Lava, M. C. Martinez, J. Ryckebusch, J. A. Caballero, and J. M. Udias, Phys. Lett. **B595**, 177 (2004), nucl-th/0401041.

- [33] B. Van Overmeire, W. Cosyn, P. Lava, and J. Ryckebusch, Phys. Rev. **C73**, 064603 (2006), nucl-th/0603013.
- [34] B. Van Overmeire and J. Ryckebusch, Phys. Lett. **B644**, 304 (2007), nucl-th/0608040.
- [35] M. C. Martinez, P. Lava, N. Jachowicz, J. Ryckebusch, K. Vantournhout, and J. M. Udias, Phys.Rev. **C73**, 024607 (2006), nucl-th/0505008.
- [36] R. J. Glauber, *Lectures in Theoretical Physics* (Interscience, New York, 1959).
- [37] R. J. Furnstahl, B. D. Serot, and H.-B. Tang, Nucl. Phys. **A615**, 441 (1997), nucl-th/9608035.
- [38] T. Bauer, R. Spital, D. Yennie, and F. Pipkin, Rev. Mod. Phys. **50**, 261 (1978).
- [39] S. Frankel, W. Frati, and N. Walet, Nucl. Phys. **A580**, 595 (1994), nucl-th/9301011.
- [40] R. Roth, T. Neff, and H. Feldmeier, Prog. Part. Nucl. Phys. **65**, 50 (2010), 1003.3624.
- [41] L. L. Frankfurt and M. I. Strikman, Phys. Rept. **160**, 235 (1988).
- [42] M. Arneodo et al. (New Muon Collaboration), Nucl.Phys. **B429**, 503 (1994).
- [43] M. Derrick, D. Krakauer, S. Magill, D. Mikunas, B. Musgrave, J. Repond, R. Stanek, R. Talaga, H. Zhang, R. Ayad, et al. (ZEUS Collaboration), Phys.Lett. **B356**, 601 (1995), hep-ex/9507001.
- [44] S. Aid, V. Andreev, B. Andrieu, R.-D. Appuhn, M. Arpagaus, A. Babaev, J. Bhr, J. Bn, Y. Ban, P. Baranov, et al. (H1 Collaboration), Nucl.Phys. **B468**, 3 (1996), hep-ex/9602007.
- [45] O. Buss, T. Gaitanos, K. Gallmeister, H. van Hees, M. Kaskulov, O. Lalakulich, A. Larionov, T. Leitner, J. Weil, and U. Mosel, Physics Reports **512**, 1 (2012), ISSN 0370-1573.
- [46] <http://gibuu.physik.uni-giessen.de/GiBUU>.